EGYPTIAN JOURNAL OF BOTANY (EJBO)

Print ISSN: 0375-9237
Online ISSN: 2357-0350

Eco-friendly synthesis of *Lactobacillus acidophilus*-AgNPs: a novel approach to combat lipid metabolism disorders

Abeer S. Elgamassy, Mohammed A. Hussein, Rafaat M. Elsanhoty, Abeer A. Mohammed

PUBLISHED BY
THE EGYPTIAN
BOTANICAL SOCIETY

Eco-friendly synthesis of *Lactobacillus acidophilus*-AgNPs: a novel approach to combat lipid metabolism disorders

Abeer S. Elgamassy[1,2], Mohammed A. Hussein[1], Rafaat M. Elsanhoty[5], Abeer A. Mohammed[2]

[1]*Department of Biotechnology, Faculty of Applied Health Sciences Technology, October 6 University, Egypt*
[2]*Department of Microbial Biotechnology, Genetic Engineering and Biotechnology Research Institute, University of Sadat City, Sadat City, Egypt*
[3]*Department of Industrial Biotechnology, Genetic Engineering and Biotechnology Research Institute, University of Sadat City, Sadat City, Egypt*

Multiple strains of lactic acid bacteria have evolved mechanisms to withstand metal ion toxicity by generating lactic acid bacteria biomass-metal nanoparticles. *Lactobacillus acidophilus* (*L. acidophilus*), a well-known probiotic, has been extensively studied for its antioxidant, cholesterol-lowering, and anti-inflammatory properties. While silver nanoparticles (AgNPs) have various applications, the use of *L. acidophilus* biomass in AgNP synthesis, particularly in lipid metabolism and inflammation, requires careful evaluation. Our study focused on the synthesis and characterization of *L. acidophilus*-AgNPs and their lipid-lowering effects in high-fat diet (HFD)-induced obese mice. The isolated *L. acidophilus* was characterized using bile salt tolerance, cell-surface adherence, hemolytic testing, and 16S rDNA sequencing. We performed an MTC test to determine the most effective Ag+ concentration for biosynthesis, finding 2 mM to be optimal and harmless. We employed TAM, DLS, UV, and FT-IR methodologies to analyze *L. acidophilus*-AgNPs, which exhibited a spherical morphology with an average particle size of 18.69 ± 0.57 nm and a PDI of 0.54. The zeta potential was -9.55 ± 0.8 mV. UV-visible and FTIR spectra revealed OH, C=O, NH, P-O, and P=O as main functional groups in the proteins and polysaccharides of *L. acidophilus*. *L. acidophilus*-AgNPs demonstrated notable lipid-lowering, antioxidant, and anti-inflammatory effects in HFD-induced obese mice. Administration of *L. acidophilus*-AgNPs significantly reduced plasma glucose by 14.72% and insulin levels by 20.18% at a dose of 17 mg/kg.b.w., and by 20.52% and 32.80%, respectively, at a dose of 42.5 mg/kg.b.w. Additionally, plasma total cholesterol (TC) and triglycerides (TG) were reduced by 16.09% and 20.65%, respectively, at the higher dose. The levels of hepatic oxidative stress markers, including MDA, were reduced by 62.42%, while antioxidant enzymes such as GSH, SOD, GPx, and GR was significantly elevated. Histological studies corroborated these biochemical findings, showing improved liver morphology in treated mice. In conclusion, *L. acidophilus* biomass can produce *L. acidophilus*-AgNPs, showcasing these bacteria as a natural microbial cell nanofactory. This method offers a sustainable and environmentally friendly approach to synthesizing *L. acidophilus*-AgNPs. The results suggest that *L. acidophilus*-AgNPs may be more effective in restoring antioxidant status in obese mice compared to metformin, rapidly counteracting lipid peroxidation and reducing obesity-related complications.

Keywords: Rice; Mannitol; NaCl; ROS; Antioxidants enzymes; Gene expression

ARTICLE HISTORY
Submitted: February 02, 2025
Accepted: April 25, 2025

CORRESPONDENCE TO
Mohammed A. Hussein,
Department of Biotechnology,
Faculty of Applied Health Sciences
Technology, October 6 University, Egypt
E-mail: prof.husseinma@o6u.edu.eg
DOI: 10.21608/ejbo.2025.357377.3172

EDITED BY: N. Khalil

INTRODUCTION

The accumulation of adipose tissue results in obesity, a chronic metabolic illness that has multiple causes (WHO, 2022). WHO reports indicate that approximately 2.5 billion individuals worldwide are overweight, with 890 million classified as obese (WHO, 2022). Several studies have observed the relationship between obesity and type 2 diabetes mellitus (DM2), high blood pressure, abnormal levels of plasma lipids, and obstructive sleep apnea syndrome (Hussein and Abdel-Gawad, 2010; Shehata *et al*., 2015). In addition, other reports have found a strong correlation between obesity and susceptibility to specific types of tumors, including those affecting the colon, rectum, post-menopausal breast, endometrial, kidneys, esophagus, and pancreas (Hussein and soad,2010;Mohamad *et al.*, 2022). On the other hand, the lipid profile, quantity, and quality of lipoproteins were dramatically changed in obese patients with hyperglycemia and insulin resistance (Hussein and soad,2010;Mohamad *et al.*, 2022). Accordingly, the production of new lipids by activating the SREBP-1 protein is promoted, and lipoprotein lipase in adipose tissue breaks down triglycerides into free fatty acids (Hussein and soad,2010;Mohamad *et al.*, 2022). Moreover, free fatty acids flow from adipocytes to the liver, which builds up viscerally, resulting in more production of VLDL and triglycerides as well as depletion of HDL-c in the liver (Boshra & Hussein, 2016; Kamal *et al*., 2022).

The FAO and WHO approve probiotics as living microbes that, when given in sufficient quantities, improve the host's health (Soliman *et al.*, 2022;Borik & Hussein, 2022). Subsequently, numerous articles have been carried out to evaluate the impact of lactic acid bacteria, particularly strains of probiotics, on reducing cholesterol levels (El-Gizawy & Hussein, 2015; Mosaad *et a*l., 2022). Other documents proved that intestinal probiotics regulated blood cholesterol levels by improving bile-salt hydrolase activity and enhancing the rate of excretion (Al-Nami *et al*., 2023). Several investigations have been carried out on the process of producing AgNPs using lactic acid bacteria (Al-Nami *et al*., 2023). Another document has also shown that *Lactobacillus acidophilus* can be used as an effective reducing agent for producing AgNPs with spherical shapes and diameters ranging from 4 to 50 nm. Similarly, several investigations have documented the use of lactic acid bacteria supernatant as a reducing agent in the manufacture of AgNPs (Hussein, 2021;Abdalla *et al*., 2023). The current investigation involved the isolation and

characterization of *L acidophilus* strains that were isolated from Yoghurt. Thus, our study was extended to optimize and characterize *L acidophilus* cell biomass-AgNPs to assess its antioxidant and lipid-lowering activity in high-fat diet (HFD)-induced obesity in mice.

MATERIALS AND METHODS

Materials

L acidophilus was purchased from the Microbial Inoculants Center at Ain Shams University in Egypt. Silver nitrate was purchased from Sigma-Aldrich (USA). It is prepared at a concentration of 10 mg in deionized water, then filter-sterilized using a disposable syringe filter with a polyethersulfone membrane pore size of 0.22 µm (from Whatman International, Maidstone, UK). de Man, Rogosa, and Sharpe (MRS) medium was used for cultivating-L acidophilus and was purchased from Sigma Aldrich. Also, all the reagents used were of analytical grade.

Culture and extraction of *L acidophilus* biomass

Culturing *L. acidophilus*: *L. acidophilus* was cultured in 100 mL of de Man, Rogosa, and Sharpe (MRS) medium and allowed overnight at 37°C, and the agitation speed was 150 rpm. Harvesting the Biomass: After the incubation period, the bacterial biomass was harvested by centrifugation at 2800 g for 10 minutes to separate the bacterial cells from the liquid supernatant. The *L. acidophilus* biomass was divided into two parts. It's common to split the biomass for further experiments or analyses. The first one into four subparts and the first subpart was used for 16S rRNA gene sequence analysis according to Cheng and Jiang (Cheng&Jiang,2016). 16S rDNA sequencing was used to identify the isolated *L acidophilus.* Briefly, the genomic DNA of the isolated *L acidophilus* was extracted using a DNA extraction kit from Qiagen, United States. The amplicons were sequenced automatically using a DNA analyzer (SeqStudio Flex DNA analyzer, Life Technologies Ltd 3 Fountain Drive Inchinnan Business Park Paisley PA4 9RF, UK).

Sequencing Setup: The sequencing was performed using an automatic sequencer, specifically the ABI PRISM 3730XL Analyzer with Big Dye TM Terminator Cycle Sequencing Kit. The protocols provided by the manufacturer were followed during the sequencing process.

Primer and Template: Single-pass sequencing was carried out for each template. The primer used was the Rbcl Forward primer. This primer binds to the template DNA and initiates the sequencing reaction. Table 1 explains the primer sequence.

Fragment Purification: After the sequencing reaction, the fluorescent-labeled fragments (generated during the sequencing process) were purified. The purification step removed any unincorporated terminators and other impurities. An ethanol precipitation protocol was likely used for purification.

Sample Resuspension and Electrophoresis: The purified samples were resuspended in distilled water. Finally, the samples were subjected to electrophoresis in an ABI 3730xl sequencer (Microgen Company). Electrophoresis separates the DNA fragments based on size, allowing for the determination of the DNA sequence. The whole 16S rDNA data and the phylogenetic tree were produced using the BLAST software program. Sequence similarity searches were compared with NCBI (https://www.ncbi.nlm.nih.gov/nuccore/OR673306.1/#, accessed on 20-OCT-2023) database.

The estimation of bile salt tolerance

The bile salt tolerance estimation of *L. acidophilus* was determined using the second subpart according to the method of Leite et al, (Leite *et al.*, 2015) with some modifications. Briefly, an overnight culture of *L. acidophilus* grew. The initial cell concentration was 10^8 CFU/ml. The culture was harvested by centrifugation at 10,000 rpm for 5 minutes. The cells were then resuspended in PBS (pH 6.5), with an absorbance of 0.5 at 600 nm. Cell suspensions were adjusted to different bile salt concentrations: 0.05%, 0.05, 0.15, 0.20, 0.25, 0.30% (w/v) oxgall (w/v) oxgall (Difco, Detroit, MI, USA). and incubated at 37°C for 1, 2, and 3 hours. After incubation, viable cells were enumerated. The enumeration was performed on MRS agar plates. Two sets of plates were prepared: one with a bile (oxgall) and one without bile (control). The percentage of *L. acidophilus* survival rate was calculated using Equation (1). This survival rate reflects how well the bacteria tolerated the bile exposure.

$$\text{Survival rate } (\%) = [\log A_1 / \log A_0] \times 100$$

Where: A_1 = Final (Log CFU/mL)

A_0 = Initial (Log CFU/mL)

Assay the cell surface adhesion to solvents.

The cell surface hydrophobicity assay of *L. acidophilus* was determined using the third subpart according to the method of Abbasiliasi et al. (Sahar Abbasiliasi *et*

al., 2017). Briefly, *L acidophilus* (10^8 CFU ml/L) was created in PBS (pH 7.2) and 1 mL organic solvents (n-hexadecane chloroform and ethyl acetate). Exactly 5 mL of *L acidophilus* suspension was vortexed for 1 min and then standing for 5–10 min, the aqueous phase was isolated, and absorbance was measured at zero and after 10 min of incubation at 37 °C using Shimadzu UV-visible spectrophotometer (600 nm). Cell surface adhesion to solvents (affinity %) was expressed using the equation below:

Affinity (%) = (1- [A_1/A_0]) x 100
Where:
A_0 = absorbance of the *L acidophilus* suspension at zero time
A_1 = absorbance of the *L acidophilus* suspension after 10 min.

Assay the hemolytic activity of *L acidophilus.* **The hemolytic test for *L. acidophilus* described by** Leite et al. (Sahar Abbasiliasi *etal.*,2017). involved incubating 50 µL of a 10^8 CFU/mL *L. acidophilus* suspension on blood agar plates containing sheep blood (5% w/v) for 48 hours at 37°C. The results were then observed for signs of different types of hemolysis:

- β-hemolysis: Clear zones around colonies.
- α-hemolysis: Green-hued zones around colonies.
- γ-hemolysis: No zones around colonies.

This test helps determine the ability of the bacterium to lyse red blood cells.

Maximum Tolerable Concentration (MTC) of *L acidophilus* towards Ag^+

The MTC of *Lactobacillus acidophilus* toward Ag^+ ions was estimated as described by Presentato et al with some modifications. Briefly, a 100 mL aqueous solution containing different concentrations of Ag^+ ions (0, 1, 2, 4, 6, and 8 mM) was prepared using deionized distilled water. 2 g of *L. acidophilus* biomass was suspended in the Ag^+ solution then incubated overnight at 37 °C. After incubation, a spot-plating technique was used to assess cell viability. The diluted suspensions were spotted onto MRS agar plates (one for each tube), and then the plates were examined for bacterial growth. The experiments were performed in triplicate for accuracy.

Biosynthesis of *L acidophilus* AgNPs

This biosynthesis method allows for sustainable and eco-friendly production. The second part of *L. acidophilus* (2 g of wet biomass) was washed with phosphate-buffered saline (PBS) for biosynthesizing *L acidophilus*-AgNPs based on the method described by Thomas et al. (2014) and and Markus et al. (2016) with some modifications. Briefly, *L. acidophilus* (2 g of wet biomass) was suspended in 100 mL of $AgNO_3$ (2 mM) and then incubated at 37°C for 24 hours in the dark with gentle agitation (150 rpm). After incubation, the resulting solution turned dark brown due to the formation of AgNPs. The solution was centrifuged at high speed (18000 × g for 30 minutes) to separate the biomass and collect the biosynthesized AgNPs. The dark brown biomass was washed with buffer to remove any residual $AgNO_3$. The washed biomass was resuspended in sterilized deionized water and then ultrasonicated to disrupt the biomass cells. The suspension was centrifuged at (2800 × g for 15 minutes) to separate the AgNPs from the disrupted biomass. The pellet (containing disrupted biomass) is discarded, and the dispersed AgNPs remain in the supernatant.

Characterization of *L acidophilus* -AgNPs

The characterization methods used for the biosynthesized silver nanoparticles (AgNPs) produced from *Lactobacillus acidophilus* were described as follows:

UV-Vis Spectral Analysis: UV-Vis spectrophotometer (specifically, the UV-1800 model by Shimadzu) was employed at a wavelength range of 200–800 nm.

Transmission Electron Microscopy (TEM): A JEOL JEM-1400 TEM instrument was used at operating conditions, 120 V, and an acceleration voltage of 15 kV. Samples containing Ag nanoparticles were dispersed on a copper grid and dried at room temperature.
Particle Size Measurement: Image J software was utilized to measure the particle sizes of the AgNPs. The histogram of the size distribution was established using Origin software (version 2024).

Calculation of LD_{50} of *L acidophilus*-AgNPs

The LD_{50} of *L. acidophilus* -AgNPs was calculated as mentioned by Abal et al., method (Alamir *et al.*, 2024). Briefly, 60 mice weighing 35.5± 2.6 g. were divided into 6 groups of 10 mice in each. The groups were administered *L acidophilus*-AgNPs at 250, 500, 750, 1000, 1250, and 1500 mg/k.g.b.w.

The number of deaths within 24 hours was recorded. The LD_{50} was then calculated by the application of the following formula:

$LD_{50}=D_m-\Sigma(Z.d)/n$
Dm: The dose that killed all the mice in the group.

Z: Half the sum of the dead mice from two successive groups.
d: The difference between two successive doses.
n: The number of animals in each group.

Experimental design

The ethical guidelines (Animal Care and Use Committee of October 6th University) ensured proper care for the animals involved in the present study. Adult albino mice weighing 35 ± 2.5 grams purchased from the Faculty of Veterinary Medicine, Cairo University

Housing Conditions: Individually housed in cages, air-conditioned room with a temperature of 22 ± 2°C, relative humidity of 60%, and light cycle from 8:00 to 20:00.

Acclimatization Period: Animals were allowed to adapt to their environment. Regular diet (provided by Dyets Inc., Bethlehem, PA) was available ad libitum.

Experimental setup

This study aimed to determine the anti-obesity activity of *Lactobacillus acidophilus*-AgNPs against HFD-induced obesity in mice. The high-fat diet (HFD) used in this study consisted of the following components:

- 60% fat (primarily lard),
- 20% protein (casein),
- 20% carbohydrates (sucrose and cornstarch),
- Vitamins and minerals (standard rodent chow mix).

The HFD was administered for 8 weeks to induce obesity in the mice. As shown in Table 2, the animals were classified into five groups, with 6 mice in each.

Biochemical studies

On the 57th day, blood samples were collected from the retro-orbital venous plexus of ether-anesthetized mice (0.4 mL blood/mouse) in heparin-containing tubes and centrifuged at 1000 × g for 20 minutes for plasma separation. Plasma glucose levels were estimated calorimetrically (Fossati & Prencipe, 1982) using 6 mice per group. Plasma insulin was measured by ELISA kits (ab277390) from Abcam, UK, using 6 mice per group. Commercially available kits (Asan and Youngdong Pharmaceutical Co., Korea) were used to measure plasma total cholesterol, triglycerides, and HDL cholesterol (Allain *et al.*, 1974; Tsikas, 2017) using 6 mice per group. The liver was removed carefully, washed with saline, and divided into three sections. The first section was homogenized with phosphate buffer (pH 7.4, 1 mL), then centrifuged at 10,500 × g for 20 minutes, and the obtained supernatant was divided into two subparts. The first subpart was used to assay liver levels of TNF-α and monocyte chemoattractant protein-1 (MCP-1) using ELISA kits (E-EL-R0015, Lab Science Inc., Texas, USA) and (RAF028R, BioVendor, Czech Republic), respectively, using 6 mice per group. The second subpart was used to estimate the liver FFA content using a colorimetric assay kit (KA1667, Abnova, Taipei, Taiwan) with 6 mice per group. The second section of liver tissue was homogenized in phosphate buffer saline using 100 mg of the tissue (pH 7.4, 1 mL). The homogenate (0.2 mL) was extracted using a chloroform-to-methanol ratio of 2:1 and 1 mL, and the extract was then concentrated and used for MDA (Owen & Butterfield, 2010), GSH (Kakkar *et al.*, 1984), SOD (Maiorino *et al.*, 1995), GPx (Dym & Eisenberg, 2001), and GR (Carleton & Drury, 1980) estimation using 6 mice per group.

Histological Examination

Liver specimens were collected from 3 mice per group, fixed in 10% formalin solution, and embedded in paraffin. Fine slices (approximately 5 µm thick) were obtained from the paraffin-embedded liver specimens and stained using the H&E staining method. The stained slices were mounted on glass slides, and a light microscope was used for inspection using Bancroft and Steven's approach (Roa & Blane, 1985). Histological changes, such as fatty alterations, hepatocyte morphology, sinusoid dilation, and inflammatory cell infiltration, were scored using a semi-quantitative scoring system as follows:

Fatty Changes
0: No fatty changes.
1: Mild fatty changes (≤10% of hepatocytes affected).
2: Moderate fatty changes (10–30% of hepatocytes affected).
3: Severe fatty changes (>30% of hepatocytes affected).

Inflammatory Cell Infiltration
0: No inflammatory cells.
1: Mild infiltration (few inflammatory cells).
2: Moderate infiltration (scattered inflammatory cells).
3: Severe infiltration (dense inflammatory cell clusters).

Hepatocyte Morphology
0: Normal hepatocytes.
1: Mild changes (slight swelling or vacuolation).

2: Moderate changes (significant swelling or vacuolation).
3: Severe changes (necrosis or apoptosis).

Sinusoid Dilation

0: No dilation.
1: Mild dilation.
2: Moderate dilation.
3: Severe dilation.

The scoring was performed by two independent pathologists blinded to the treatment groups, and the average score was calculated for each parameter.

Quantitative Morphometric Analysis

To quantitatively assess morphological changes in the liver tissue, a morphometric analysis was performed using an image analysis program (ImageJ, National Institutes of Health, USA). The following parameters were measured:

Fatty Changes: The percentage area of fatty changes in the liver tissue was calculated by measuring the area of lipid droplets relative to the total tissue area in each field.

Inflammatory Cell Infiltration: The number of inflammatory cells per field (at 400× magnification) was counted and expressed as cells/mm².

Hepatocyte Morphology: The diameter of hepatocytes was measured in randomly selected fields (at 400× magnification), and the average hepatocyte size was calculated.

Sinusoid Dilation: The width of sinusoids was measured in randomly selected fields (at 400× magnification), and the average sinusoid width was calculated. For each liver specimen, 10 random fields were analyzed, and the average values were calculated. The results were compared between groups to assess the effects of *Lactobacillus acidophilus*-AgNPs on HFD-induced morphological changes.

Statistical analysis

For comparisons between multiple groups, two-way ANOVA was used, followed by Tukey's post hoc test to identify specific differences between groups. Statistical significance was set at $p < 0.05$. All analyses were performed using SPSS version 20 (IBM Corp., USA) (Altermann *et al*., 2005).

RESULTS

16s rRNA identification of *L acidophilus*

To determine the identity of the isolated *L acidophilus*, we employed phylogenetic analysis in our work. The task was carried out by BLAST. Figure 1 shows that the maximal sequence similarity of a 1500 bp fragment of the 16S rRNA gene used for genotypic identification by gene sequencing was 99.35% to the GenBank reference strain *Lacidophilus* with accession number(https://www.ncbi.nlm.nih.gov/nuccore/OR673306 .1/#, accessed on October 20, 2023) that is available online. Furthermore, the *L acidophilus* that was examined showed positive results with a size of 1500 bp after agarose gel electrophoresis of amplified PCR products (Figure 2). PCR produced the expected 0.9K amplicons, and a partial 16S rRNA sequencing analysis of *L acidophilus* showed 99% identity.

Bile Salt Tolerance Test

The isolated *L acidophilus* was subjected to different oxgall concentrations, 0.10-0.30%, at incubation times of 1, 2, and 3 h. As shown in Figure 3, the isolated *L. acidophilus* conferred the highest survival rate (%) of more than 80% at 0.25 and 0.30% bile concentrations after incubation for one hour. At the same oxgall concentration (0.25 and 0.30% bile), there were no significant changes in survival rate (%) at 1-, 2-, and 3-hour incubation.

Assay of *L acidophilus* affinity *to* solvents

The findings from Figure 4 appear that *L. acidophilus* exhibits varying affinities to different solvents, and this affinity changes over time. *L. acidophilus* has the highest affinity for ethyl acetate, followed by n-hexadecane, and then chloroform. As time increases (10-, 20-, 30-, and 40-minute incubation), the affinity of *L. acidophilus* to the solvents also increases. This suggests that the *L. acidophilus* interaction with the solvents becomes stronger over time. Hydrophobicity and Lewis acid-base characteristics play a crucial role in *L. acidophilus* adhesion to surfaces. Hexadecane, a polar solvent, was used to evaluate the hydrophobicity or hydrophilicity of the cell surface. Ethyl acetate (a basic solvent and electron donor) and chloroform (an acidic solvent and electron acceptor) were used to explore Lewis's acid-base characteristics.

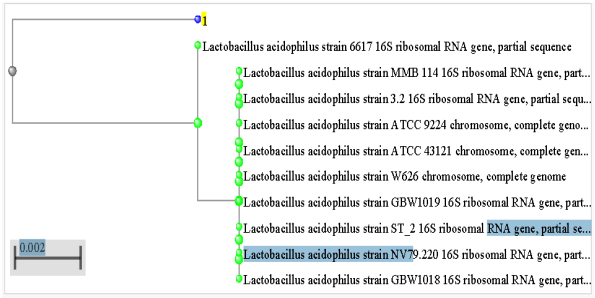

Figure 1. Phylogenetic tree using BLAST "NCBI, U.S." of *L acidophilus* strains using *16S rRNA,* showing names of bacteria species and accession numbers.

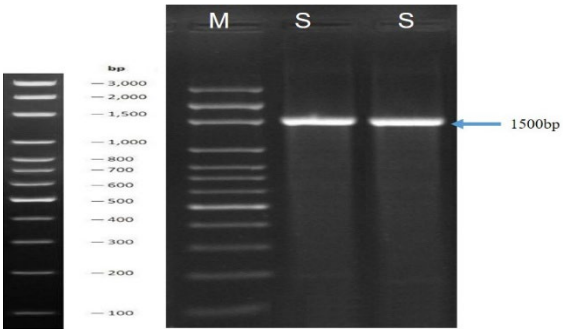

Figure 2.The bands corresponding to the amplified sequences in the PCR reaction (M: DNA ladder: 50 bp, S: band *L acidophilus*, about 1500 bp.)

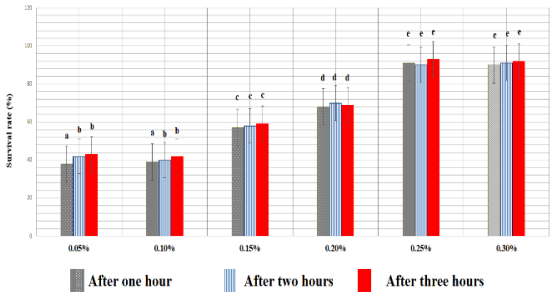

Figure 3. Survival rates of *L acidophilus* in bile salt (0.05 – 0.30%) conditions for 1, 2, and 3 hs. Values represent the mean ± SD (n=3). Data followed by the same letter are not significantly different at P ≤ 0.05.

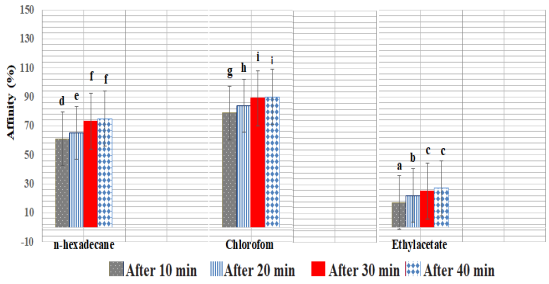

Figure 4. Adhesion assay of *L acidophilus* to solvents (n-hexadecane chloroform and ethyl acetate). Values represent the mean ± SD (n=3). Data followed by the same letter are not significantly different at P ≤ 0.05.

Hemolytic activity of *L. acidophilus*

Hemolysis is a process where microorganisms break down red blood cells, releasing hemoglobin. There are three main types of hemolysis:

- α-hemolysis: Partial hemolysis, resulting in a greenish discoloration around bacterial colonies.
- β-hemolysis: Complete hemolysis, leading to a clear zone around bacterial colony.
- γ-hemolysis: No hemolysis, with no change in the appearance of the agar around bacterial colonies.

In the current investigation *L. acidophilus* was tested for hemolysis on agar blood plates. The results indicated that *L. acidophilus* did not exhibit any hemolysis on these plates. This absence of hemolysis suggests that *L. acidophilus* does not cause damage to red blood cells. The fact that *L. acidophilus* was γ-hemolytic (no hemolysis) aligns with its non-pathogenic nature.

MTC value of *L. acidophilus* towards Ag^+

The data presented in Figure 5 regarded the UV-visible spectra and the formation of silver nanoparticles (AgNPs):

Control (No AgNPs): The UV-visible spectra for the control (no AgNPs) did not show any absorption peak in the range of 400 to 500 nm. This absence of absorption suggests that there were no AgNPs present in the control sample.

Absorption Spectra with AgNPs: At a concentration of 2 mM, a narrow absorption spectrum was observed with a main band centered at 460 nm. This specific wavelength corresponds to the surface plasmon resonance (SPR) of AgNPs. Additionally, at concentrations of 1 mM and 2 mM, broad absorption spectrum was observed: Main bands were centered at 425 nm and 430 nm, respectively. At concentrations of 4 and 6 mM, another broad absorption spectrum was observed: Main bands were centered at 450 nm and 470 nm, respectively to indicate the formation of AgNPs.

Absorbance Trends: The absorbance increased as the concentration of $AgNO_3$ (silver nitrate) reached 2 mM. However, the absorbance decreased at higher concentrations (4 mM, 6 mM, 1 mM, and 8 mM). The UV-visible spectra provide valuable insights into the presence and characteristics of AgNPs. The specific SPR peak at 460 nm confirms the formation of AgNPs, while the broader bands at other wavelengths also support this conclusion.

Characterization of *L-acidophilus*-AgNPs

Figures 6 a and b show TEM and DLS micrographs of biosynthesized *L acidophilus*-AgNPs. These show clear, sphere-shaped nanoparticles that are smooth. Also, the average vesicle size of *L acidophilus*-AgNPs was 18.69 ± 0.57 nm, with a polydispersity index (PDI) of 0.54, indicating a narrow particle size distribution. The measured zeta potential value of *L acidophilus*-AgNPs was -9.55 ± 0.8 mV. Figure 7 shows the UV-Vis. absorption spectra of crude *L acidophilus* biomass and *L acidophilus*-AgNPs. *L. acidophilus* biomass exhibited one characteristic band at 240 nm indicating the presence of protein and polysaccharides. Absorption spectra attribute sharp surface plasmon resonance (SPR) to two bands characteristic of *L. acidophilus* -AgNPs at 245 and 430 nm. The FT-IR spectra of both crude *L. acidophilus* biomass and *L. acidophilus* -AgNPs are provided in Figures 8 and 9. These spectra offer valuable insights into the functional groups present in these samples:

Crude *L. acidophilus* Biomass: The FT-IR spectrum of crude *L. acidophilus* biomass revealed several characteristic peaks associated with different functional groups:

- 3429 cm^{-1} (OH): Represents hydroxyl groups.
- 2989 cm^{-1} (C-H stretching vibration): Indicates aliphatic hydrocarbon bonds.
- 2851 cm^{-1} (CH-aliph.): Corresponds to aliphatic carbon-hydrogen bonds.
- 1593 cm^{-1} (C=O): Represents carbonyl groups.
- 1542 cm^{-1} (Amide II): Involves N-H bending in primary amides and C-N stretching in secondary amides.
- 1473 cm^{-1} (C=C-stretching): Indicates carbon-carbon double bonds.
- 1340 cm^{-1} (C-O bending): Associated with bending vibrations of carbon-oxygen bonds.

***L. acidophilus*-AgNPs**: The FT-IR spectra of *L. acidophilus*-AgNPs exhibited similar distinctive peaks, but their intensities varied. Notably, the presence of 1403 cm^{-1} and 1280 cm^{-1} peaks suggests:

- O-H bending and C-O stretching vibrations in the carboxylate ion group.
- These vibrations likely occur in conjunction with phosphate groups (P=O and P-O of the C-PO_3^{-2}).

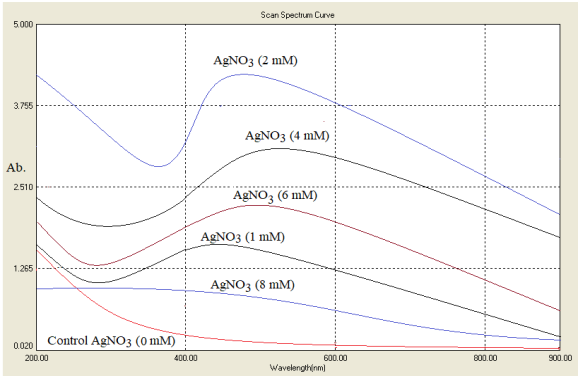

Figure 5. MTC value of *L acidophilus* towards Ag^{+} (0, 1, 2, 4, 6, and 8 mM).

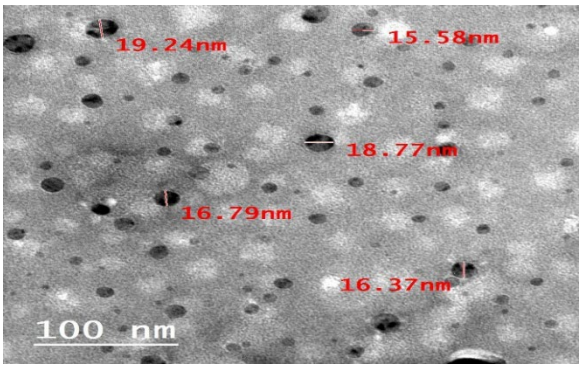

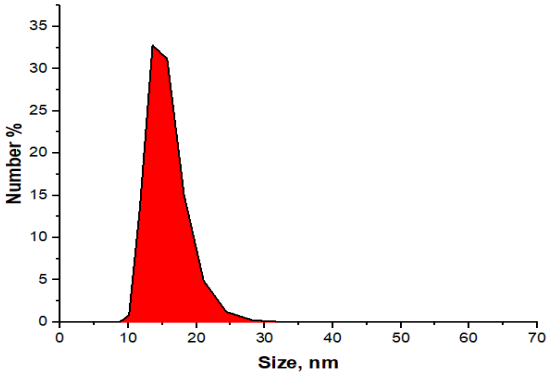

Figures 6 (a b). TEM micrographs and zeta potential, respectively of biosynthesized *L acidophilus*-AgNPs.

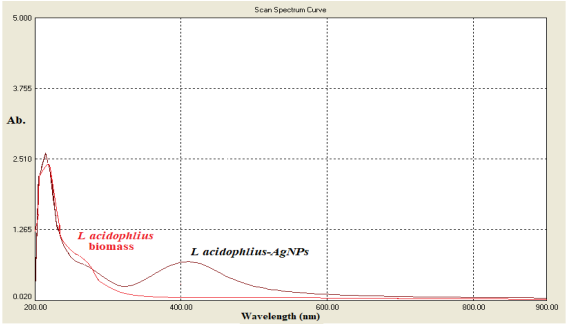

Figure 7. UV spectra of *L acidophilus* biomass (red curve) and biosynthesized *L acidophilus*-AgNPs (black curve.

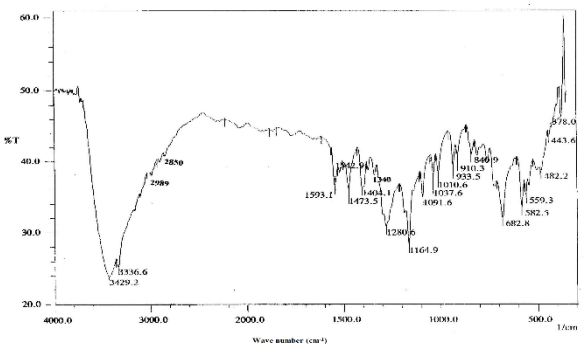

Figure 8. FTIR Spectra of *L acidophilus* biomass

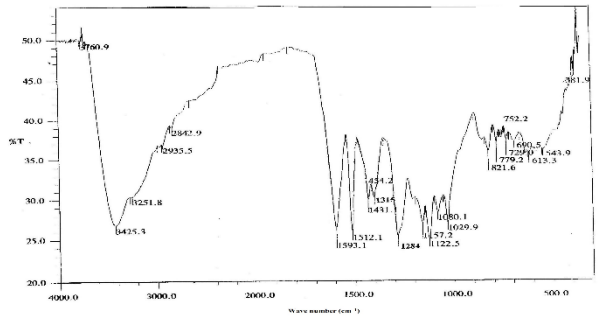

Figure 9. FTIR Spectra of biosynthesized *L acidophilus*-AgNPs.

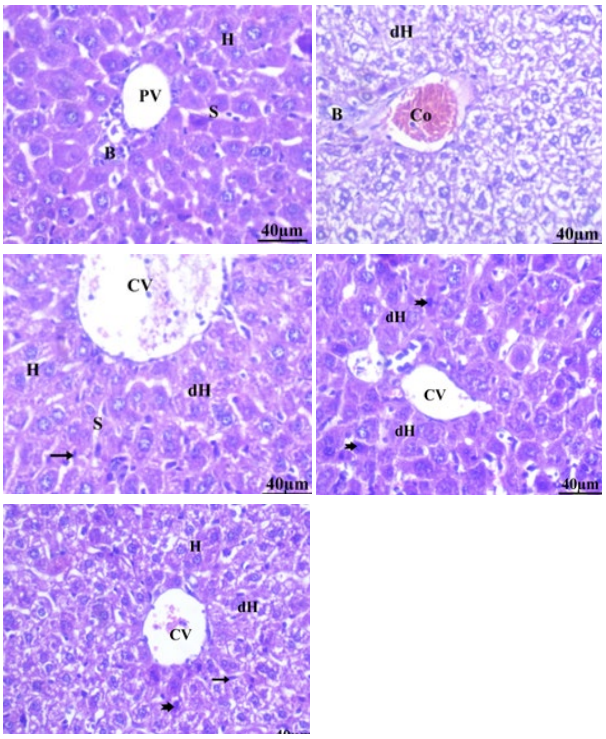

Figure 10. Microscopic pictures of H&E-stained liver sections. (a): Group I, normal group feed regular diet; (b): Group II: Was administer HFD; (c): Group III: Was administrated HFD + *L acidophilus*-AgNPs (17 mg/kg.b.w.); (d): Group IV: Wasadministratede HFD + *L acidophilus*-AgNPs (42.5 mg/kg.b.w.); (e): Was administrated HFD + metformin (500 mg/kg.b.w.).

Additionally, the 1091.9 cm^{-1} peak corresponds to the vibrations of: (C-C=O, C-O-P) phosphoprotein and hydroxyl groups derived from saccharides. Both the crude *L. acidophilus* biomass and the *L. acidophilus*-AgNPs exhibit specific functional group vibrations, providing valuable information about their composition.

Evaluation of the LD_{50} of *L-acidophilus-AgNPs*

The oral administration of *L. acidophilus*-AgNPs was tested at various doses: 250, 500, 750, 1000, 1250, and 1500 mg/kg body weight. The results indicate a dose-dependent effect: 0 deaths at 250 mg/kg, 1 death at 500 mg/kg, 5 deaths at 750 mg/kg, 7 deaths at 1000 mg/kg, 8 deaths at 1250 mg/kg, and 10 deaths at 1500 mg/kg. The lethal dose (LD50) of *L. acidophilus*-AgNPs is 850 mg/kg.

Mortality and Survival Rates

During the 8-week experimental period, the mortality and survival rates of animals in each group were recorded. The results are summarized below:

Group I (Regular Diet - RD)

- Mortality: 0% (0 out of 6 mice).
- Survival: 100%.

Group II (High-Fat Diet - HFD)

- Mortality: 16.67% (1 out of 6 mice).
- Survival: 83.33%.

Group III (HFD + *L. acidophilus*-AgNPs, 17 mg/kg.b.w.)

- Mortality: 0% (0 out of 6 mice).
- Survival: 100%.

Group IV (HFD + *L. acidophilus*-AgNPs, 42.5 mg/kg.b.w.)

- Mortality: 0% (0 out of 6 mice).
- Survival: 100%.

Group V (HFD + Metformin, 500 mg/kg.b.w.)

- Mortality: 0% (0 out of 6 mice).
- Survival: 100%.

The mortality observed in the HFD group (Group II) was likely due to complications associated with obesity and metabolic stress. No mortality was observed in the treatment groups, indicating the safety and efficacy of *L. acidophilus*-AgNPs and metformin in mitigating HFD-induced complications.

Assay the effect of *L-acidophilus-AgNPs* on mice's body weight

The current findings in Table 4 showed the changes in body weight of obese mice when treated with *L-acidophilus-AgNPs*.

Normal control Group vs. HFD-Fed Mice: The HFD-fed mice (high-fat diet) experienced a significant increase in body weight by 36.60% compared to the control group. This weight gain is likely due to the high-fat diet.

Effects of *L. acidophilus*-AgNPs and Metformin: Our study evaluated the impact of two interventions:

- L. acidophilus-AgNPs at doses of 17 mg/kg b.w. and 42.5 mg/kg b.w.
- Metformin at a dose of 500 mg.

Relative to obese mice, the following effects were observed:

- *L. acidophilus*-AgNPs (17 mg/kg b.w.): 16.48% reduction in body weight.
- *L. acidophilus*-AgNPs (42.5 mg/kg b.w.): 25.50% reduction in body weight.
- Metformin (500 mg): 32.9% reduction in body weight.

These reductions were statistically significant ($p<0.05$). Our results proved that both *L. acidophilus*-AgNPs and metformin demonstrated potential for weight reduction in HFD-fed mice.

Effects of L-acidophilus-AgNPs and metformin on plasma glucose, insulin levels in treated mice

Table 5 explains the plasma glucose and insulin levels of treated mice. When compared to normal mice, HFD-fed mice had a considerable rise ($p < 0.05$) in plasma glucose and insulin levels of 58.98 and 46.54 %, respectively. Furthermore, when compared to obese mice ($p < 0.05$), plasma levels of glucose and insulin in mice treated with *L acidophilus-AgNPs* (17 mg/kg.b.w.) were substantially reduced by 14.72 and 20.18 %, respectively. In addition, as compared to obese mice, administration of *L acidophilus-AgNPs* (42.5 mg/kg.b.w.) considerably decreased plasma glucose and insulin levels by 20.52 and 32.80%, respectively ($p < 0.05$). Furthermore, metformin reduced the blood levels of glucose and insulin by 26.51 and 35.68 %, respectively ($p < 0.05$).

Effects of *L-acidophilus*-AgNPs and metformin on plasma lipid profile and liver FFA in treated mice

The current results in Table 6 related to lipid levels and the effects of different treatments in high-fat diet-fed mice.

High-fat diet (HFD) vs. normal control group In HFD-fed mice: PlasmaTC, TG, and FFA increased by 32.39, 44.36, and 76.28%, respectively. and plasma HDL-C levels decreased by 35.08% ($p < 0.05$).

Effects of *L. acidophilus*-AgNPs and Metformin *L. acidophilus*-AgNPs (17 mg/kg b.w.): Reduced plasma TC, TG, and FFA by 10.61, 13.10, and 14.22%, respectively, and increased HDL-C by 19.71% ($p < 0.05$).

L. acidophilus-AgNPs (42.5 mg/kg b.w.): Significantly reduced TG, TC, and FFA levels by 20.65%, 16.09%, and 27.56%, respectively and elevated HDL-C by 41.01% ($p < 0.05$).

Metformin: Decreased TG, TC, and FFA levels by 26.13%, 21.84%, and 35.46%, respectively, and significantly ($p < 0.05$) elevated HDL-C by 31.26%.

Effects of *L-acidophilus*-AgNPs and metformin on hepatic MDA, GSH, SOD, GPx, and GR in treated mice

Our findings in Table 7 related to hepatic oxidative stress markers and the effects of different *L-acidophilus*-AgNPs treatments in mice feed a high-fat diet (HFD).

Hepatic Oxidative Stress Markers in HFD-Fed Mice: Compared to mice fed the normal diet: MDA levels were considerably higher by 209.07% in HFD-fed mice. Levels of GSH, SOD, GPx, and GR were significantly decreased by 68.31%, 56.57%, 73.86%, and 57.34%, respectively.

Effects of *L. acidophilus*-AgNPs and Metformin: Compared to HFD-treated mice: Administration of *L-acidophilus*-AgNPs (17 mg and 42.5 mg) and metformin significantly reduced MDA levels by 55.15%, 62.42%, and 61.83%, respectively ($p < 0.05$). Specifically, at 17 mg, *L-acidophilus*-AgNPs significantly decreased GSH, SOD, GPx, and GR levels by 120.0%, 77.63%, 146.31%, and 64.57%, respectively. At 42.5 mg, L-acidophilus-AgNPs significantly increased liver GSH, SOD, GPx, and GR by 138.8%, 102.92%, 229.83%, and 96.13%, respectively. Metformin administration significantly increased liver GSH, SOD, GPx, and GR levels by 88.54%, 76.19%, 124.95%, and 54.37%, respectively. Our findings proved that both *L. acidophilus*-AgNPs and metformin appear to modulate hepatic oxidative stress markers in HFD-fed mice.

Table 1. Primer sequence

Primer Code	Sequence	Product Size
27F	5'- AGAGTTTGATCCTGGCTAG -3'	1500 bp
1492R	5'- GGTTACCTTGTTACGACTT -3'	

Table 2. Description of treatment groups

Group	Treatment Description	Treatment Description
I	Regular diet (RD)	For 8 weeks, they received a normal diet
II	HFD	For 8 weeks, given a high-fat diet (Troisi *et al.*, 2000).
III	HFD+ *L acidophilus-AgNPs* (17 mg/kg.b.w.)	Over 8 weeks, mice were administered a high-fat diet with 1 mL (*L acidophilus-AgNPs* (17 mg/kg.b.w.).
IV	HFD+ *L acidophilus-AgNPs* (42.5 mg/kg.b.w.)	For 8 weeks, mice were fed a high-fat diet with *L acidophilus-AgNPs* (42.5 mg/kg.b.w.) suspended in distilled water orally in a single daily dose.
V	HFD + Metformin (500 mg/kg.b.w.)	For 8 weeks, mice were fed a high-fat diet with metformin. (500 mg/kg.b.w.) suspended in distilled water orally in a single daily dose (Troisi *et al.*, 2000).

Table 3. Determination of LD_{50} of *L acidophilus*-AgNPs given orally in adult mice.

Group	Dose (mg/kg)	No. of animals/group	No. of dead animals	(Z)	(d)	(Z.d)
1	250	10	0	0.5	250	125
2	500	10	1	3.0	250	750
3	750	10	5	6.0	250	1500
4	1000	10	7	7.5	250	1875
5	1250	10	8	9.0	250	2250
6	1500	10	10	000	00	6500

$$LD_{50} = Dm - \left[\frac{\sum (Z.d)}{n}\right] \qquad LD_{50} = 1500 - \left[\frac{6500}{10}\right] = 850 \text{ mg/Kg.b.w.}$$

Table 4. Changes in body weight of control and experimental groups of treated mice

No.	Groups	Number of weeks Body weight of mice(g)				
		0	2	4	6	8
(I)	Regular diet (RD)	35.5 ± 3.25^{Aa}	38.9 ± 1.51^{Ab}	42.84 ± 1.79^{Bc}	45.27 ± 2.75^{Bc}	47.11 ± 2.70^{Bd}
(II)	HFD	34.85 ± 2.80^{Aa}	39.74 ± 1.86^{Ab}	49.65 ± 3.58^{Cc}	58.50 ± 2.65^{Cd}	64.37 ± 2.11^{De}
(III)	HFD+ *L acidophilus*-AgNPs (17mg/kg.b.w.)	35.9 ± 1.23^{Aa}	39.58 ± 1.48^{Ab}	41.61 ± 2.18^{ABc}	47.9 ± 1.39^{Bd}	53.76 ± 2.90^{Ce}
(IV)	HFD+ *L acidophilus*-AgNPs (42.5mg/kg.b.w.)	35.54 ± 1.68^{Aa}	37.83 ± 3.26^{Aa}	42.66 ± 3.52^{Bb}	45.84 ± 3.15^{Bc}	47.94 ± 3.9^{Bc}
(V)	HFD + Metformin (500 mg/kg.b.w.)	35.60 ± 2.87^{Aa}	37.64 ± 2.75^{Aab}	39.05 ± 3.10^{Abc}	41.63 ± 2.45^{Ac}	43.18 ± 2.86^{Ad}

The body weight of mice consuming regular and high-fat as well as high-fat diet, plus *L acidophilus*-AgNPs (17, and 42.5 mg/kg.b.w.) and Metformin (500 mg/kg.b.w.) during the 8 weeks. Values are given as mean ± SD significantly different at $P \leq 0.05$ for groups of eight animals each. Small letters are used for comparison between the means within the column. Capital letters are used to compare means within the row.

Table 5. Effect of *L acidophilus*-AgNPs, and metformin on plasma glucose and insulin in treated mice

No.	Groups	Glucose (mg/dl)	Insulin (ng/mL)
(I)	Regular diet (RD)	100.93 ± 8.27^{a}	1.34 ± 0.11
(II)	HFD	160.46 ± 6.30^{a}	2.13 ± 0.12^{a}
(III)	HFD+ *L acidophilus-AgNPs* (17 mg/kg.b.w.)	136.84 ± 4.03^{a}	1.70 ± 0.07^{a}
(IV)	HFD+ *L acidophilus-AgNPs* (42.5 mg/kg.b.w.)	127.53 ± 6.07	1.43 ± 0.05^{b}
(V)	HFD + Metformin (500 mg/kg.b.w.)	117.91 ± 4.56	1.37 ± 0.04

Values represent the mean ± SE (n=6). Data shown are mean ± standard deviation of the number of observations within each treatment. Data followed by the same letter are not significantly different at $P \leq 0.05$.

Effects of *L-acidophilus*-AgNPs and metformin on liver TNF-α and MPC-1 in treated mice

Our investigations reported in Table 8 related to hepatic levels of TNF-α and MCP-1 in mice fed a high-fat diet (HFD). TNF-α and MCP-1 are pro-inflammatory cytokine involved in immune responses and inflammation. In HFD-fed mice, hepatic expression of TNF-α, and MCP-1 dramatically increased by 166.89 and 389.67 %, respectively, compared to normal mice ($p<0.05$). However, when obese mice were treated with *L-acidophilus*-AgNPs (17 mg): TNF-α and MCP-1 levels decreased by 58.92, and 42.31%, respectively compared to HFD-treated mice ($p<0.05$). In addition, when obese mice were treated with *L-acidophilus*-AgNPs (42.5 mg)TNF-α and MCP-1 levels decreased by 63.41, and 75.31%, respectively compared to HFD-treated mice ($p<0.05$). Moreover, when obese mice were treated with Metformin TNF-α and MCP-1 levels decreased by 49.24, and 70.25%, respectively compared to HFD-treated mice ($p<0.05$). Our findings proved that both L-acidophilus-AgNPs and metformin modulate hepatic inflammation by reducing TNF-α and MCP-1 levels in HFD-fed mice.

Effects of *L-acidophilus*-AgNPs and metformin on liver histology in treated mice

Histopathological examination of liver sections of the normal group (I) showed within normal lobular arrangement of liver tissue. The hepatocytes (H) exhibited polygonal morphology, including acidophilic cytoplasm and centrally positioned vesicular spherical nuclei with prominent nucleoli. Also, the hepatic sinusoids (S) were seen as irregular circulatory compartments bordered by flat endothelial cells (arrow) within the hepatocyte cords. The portal tract portions contained ramifications of the portal vein (PV) and bile duct (B) (table 9 and Figure 10a). On the other hand, in the liver tissue of the HFD-fed mice group (II), histological examination showed moderate congestion in both central and portal veins may suggest impaired blood flow within the liver, which can have various causes such as inflammation, or vascular issues. Fatty changes indicate the presence of lipid accumulation in some regions of the liver tissue. (Table 9 and Figure 10b). Also, the histological results of *L-acidophilus*-AgNPs (17 mg)-treated mice indicate the presence of a small number of fatty alterations present dotted arrow). Several hepatic cells exhibited a normal and undamaged morphology, including intact form (H), sinusoids (S), and Kupfer cells (arrow). Additional hepatocytes had nuclei that were stained with a dark color (shown by a notch arrow) (table 9 and Figure 10c). In addition, we noticed that the liver region had exhibited noticeable improvement in *L-acidophilus*-AgNPs (42.5 mg) treated mice. Normal hepatocytes (H), sinusoids (S), and Kupffer cells (arrow) were seen. Specific regions of the liver tissue showed hepatocytes with karyolitic characteristics (wavy arrow), megakaryocytes (bold arrow), and pyknotic nuclei (notch arrow). There was a slight level of dilated sinusoid (dS) found. The observation indicated a moderate level of fatty alterations (dotted arrow) (table 9 and Figure 9d). Moreover, histological examination showed that the liver region has demonstrated observable improvement in structures including normal hepatocytes (H), sinusoids (S), and Kupffer cells (arrow) in obese mice treated with metformin. In addition to a slight level of fatty degeneration (dotted arrow). Certain liver cells displayed signs of cellular degeneration (dH). A small proportion of the liver cells exhibited pyknosis (notch arrow) and megakaryocytes (bold arrow) (table 9 and Figure 10e).

Quantitative Morphometric Analysis

The morphometric analysis revealed significant differences in liver morphology between the treatment groups:

Fatty Changes: The percentage area of fatty changes was significantly higher in the HFD group (32.5 ± 3.2%) compared to the control group (2.1 ± 0.5%). Treatment with *L. acidophilus*-AgNPs (42.5 mg/kg.b.w.) significantly reduced fatty changes to 12.4 ± 1.8% ($p < 0.05$).

Inflammatory Cell Infiltration: The number of inflammatory cells was significantly higher in the HFD group (45.6 ± 5.3 cells/mm²) compared to the control group (5.2 ± 1.1 cells/mm²). Treatment with *L. acidophilus*-AgNPs (42.5 mg/kg.b.w.) significantly reduced inflammatory cell infiltration to 18.7 ± 2.4 cells/mm² ($p < 0.05$).

Hepatocyte Morphology: The average hepatocyte diameter was significantly larger in the HFD group (25.3 ± 2.1 µm) compared to the control group (15.4 ± 1.2 µm). Treatment with *L. acidophilus*-AgNPs (42.5 mg/kg.b.w.) restored hepatocyte diameter to 18.6 ± 1.5 µm ($p < 0.05$).

Sinusoid Dilation: The average sinusoid width was significantly greater in the HFD group (8.7 ± 0.9 µm) compared to the control group (4.2 ± 0.5 µm). Treatment with *L. acidophilus*-AgNPs (42.5 mg/kg.b.w.) reduced sinusoid width to 5.8 ± 0.6 µm

Table 6. Effect of *L acidophilus*-AgNPs and Metformin on plasma cholesterol, triglycerides, and cholesterol-high density lipoprotein (HDL) as well as liver free fatty acids (FFA) in treated mice.

No.	Groups	Cholesterol (mg/dl)	Triglycerides (mg/dl)	HDL-C (mg/dl)	FFA (nmol/g tissue)
(I)	Regular diet (RD)	157.79± 14.74	106.91± 10.12	45.971± 4.29 ^{d}	60.94± 3.78 ^{a}
(II)	HFD	208.44±10.72	154.34±8.45 ^{c}	29.84±3.14 ^{a}	107.43±8.93 ^{d}
(III)	HFD+ *L acidophilus*-AgNPs (17 mg/kg.b.w.)	186.32± 12.11 ^{e}	134.11± 9.83	35.72± 1.81 ^{a}	92.15± 7.04 ^{d}
(IV)	HFD+ *L acidophilus*-AgNPs (42.5 mg/kg.b.w.)	166.25±6.34 ^{d}	129.24±5.53 ^{b}	42.08±2.85 ^{bc}	77.82± 5.04 ^{b}
(V)	HFD + Metformin (500 mg/kg.b.w.)	153.97 ± 9.38 ^{b}	121.73± 5.02 ^{a}	39.17± 2.56 ^{cd}	69.33± 7.89 ^{a}

Values represent the mean ± SE (n=6). Data shown are mean ± standard deviation of the number of observations within each treatment. Data followed by the same letter are not significantly different at P ≤ 0.05.

Table 7. Effect of L acidophilus-AgNPs and metformin on hepatic malondialdehyde (MDA), reduced glutathione (GSH), superoxide dismutase (SOD), glutathione peroxidase (GPx) and glutathione reductase (GR) in treated mice.

No.	Groups	MDA (n mol/g tissue)	GSH (nmol/mg tissue)	SOD (U/mg tissue)	GPx (U/mg tissue)	GR (U/mg tissue)
(I)	Regular diet (RD)	38.70± 3.52 ^{a}	2.84± 0.18 ^{e}	487.96± 17.04	19.17± 1.87	48.5± 3.53
(II)	HFD	119.61± 6.46 ^{e}	0.90± 0.09 ^{a}	211.92± 11.97 ^{a}	5.01± 0.37	20.69± 2.70
(III)	HFD+ *L acidophilus*-AgNPs (17mg/kg.b.w.)	53.64± 3.85 ^{e}	1.98± 0.20	376.45± 14.59	12.34± 1.18	34.05± 2.99
(IV)	HFD+ *L acidophilus*-AgNPs (42.5mg/kg.b.w.)	40.16± 2.41 ^{c}	2.15± 0.21	430.02± 21.19	16.53± 1.03	40.58± 2.14
(V)	HFD + Metformin (500 mg/kg.b.w.)	45.65± 4.83 ^{b}	1.70± 0.11	373.40± 11.76	11.27±0.99	31.94±2.48

Values represent the mean ± SE (n=6). Data shown are mean ± standard deviation of number of observations within each treatment. Data followed by the same letter are not significantly different at P ≤ 0.05.

Table 8. Effect of *L acidophilus*-AgNPs and metformin on liver TNF-α and monocytes chemoattractant protein-1 (MPC-1) in treated mice

No.	Groups	TNF-α (pg/g tissue)	MCP-1 (Pg/g tissue)
(I)	Regular diet (RD)	77.46± 5.05	20.91± 2.84
(II)	HFD	206.74± 16.33 ^{e}	102.39± 6.65
(III)	HFD+ *L acidophilus*-AgNPs (17 mg/kg.b.w.)	84.92± 8.09	59.06± 3.14
(IV)	HFD+ *L acidophilus*-AgNPs (42.5 mg/kg.b.w.)	75.64± 6.21	25.17± 2.42
(V)	HFD + Metformin (500 mg/kg.b.w.)	115.28± 8.30	30.57± 3.64

Values represent the mean ± SE (n=6). Data shows mean ± standard deviation of the number of observations within each treatment. Data followed by the same letter are not significantly different at P ≤ 0.05.

Table 9. Effect of *L acidophilus*-AgNPs and metformin on liver histopathological changes in HFD-treated mice

No.	Groups	Congestion	Lymphatic infiltration	Fatty degeneration	Hepatocyte degeneration
(I)	Regular diet (RD)	-	-	-	-
(II)	HFD	++	++	+++	+++
(III)	HFD+ *L acidophilus*-AgNPs (17mg/kg.b.w.)	++	++	++	++
(IV)	HFD+ *L acidophilus*-AgNPs (42.5mg/kg.b.w.)	-	+	+	+
(V)	HFD + Metformin (500 mg/kg.b.w.)	-	+	+	+

Scoring: (-) indicates normal, (+) indicates mild, (++) indicates moderate, (+++) indicates high.

($p<0.05$). These results demonstrate that *L. acidophilus*-AgNPs effectively ameliorated HFD-induced morphological changes in the liver tissue.

DISCUSSION

Lactobacillus strains are nonpathogenic microorganisms that produce lactic acid. They are widely used in dairy industries, particularly in cheese-making and yogurt production. These strains can positively impact health by altering the intestinal environment, reducing lactose intolerance, and enhancing the immune system (Hussein and Boshra, 2013). The current study explored *L. acidophilus* -AgNPs as a promising biological formula for medical applications related to obesity and its metabolic complications (Al-nami et al., 2023). The 16S rRNA sequences of *L. acidophilus* were evaluated and uploaded to Genbank for reference. Additionally, *L. acidophilus* was identified using agarose gel electrophoresis of amplified PCR products (Hussein *et al.,* 2023). Also, Elharrif et al., 2024, identified various probiotic parameters, including bile salt hydrolases and beta-galactosidases. These parameters contribute to lowering cholesterol levels and improving lactose intolerance in the host (Salah et al., 2024). Our study confirms the good survival rate of *L. acidophilus*, emphasizing its probiotic potential.

Surface Characteristics and Affinity: *Lactobacilli* strains exhibit a hydrophobic surface character (>50%). Results indicate that these strains are not highly acidic (less than 40% affinity to ethyl acetate) and are very basic (60–90% affinity to chloroform), similar to *L. acidophilus* (Altermann *et al*., 2005 and Hussein *et al.,* 2024). Most sticky probiotic lactobacilli strains possess basic and electron-donating properties, making them more attracted to chloroform than other molecules (Azcarate-Peril *et al.,* 2004). *L. acidophilus* has been extensively studied through in vitro experiments, revealing several probiotic characteristics: it can withstand low pH levels, which is crucial for its survival in the acidic environment of the gastrointestinal tract (Claesson *et al.,* 2007). It shows resistance to bile, an essential feature for its functionality in the gut. *L. acidophilus* can attach to human colon cells in cell culture, promoting beneficial interactions (Altermann *et al.*, 2005). It generates antibiotics, contributing to its protective effects (Borik and Hussein, 2021). *L. acidophilus* produces lactase, aiding in lactose digestion. It remains stable during production and storage. Hemolysis was associated with pathogenic bacteria and assessed for safety (Azcarate-Peril *et al.,* 2004). In vitro tests revealed that *L. acidophilus* from curd did not exhibit alpha or beta hemolysis. This aligns with previous findings that *L. acidophilus* strains generally lack hemolytic activity (Abdalla *et al.,* 2023). The application of bacteria in medical nanotechnology has gained attention as an alternative approach. The synthesis of nanoparticles (NPs) depends on the bacteria's ability to reduce metal ions into respective metal NPs under metal stress (Hussein *et al.,* 2023). Some bacteria, including L. acidophilus, have documented potential for metal NP synthesis (Kalimuthu *et al.,* 2008; Panáček *et al.,* 2006). MTC (Minimum Tolerable Concentration) and Ag+ Interaction: The cell biomass of L. acidophilus exhibited an MTC towards Ag+ at 2 mM, as observed from the absorption spectrum. This suggests that *L. acidophilus* can tolerate a certain concentration of silver ions (Ag+). Formation of *L. acidophilus* -AgNPs: UV-visible spectroscopy confirmed the formation of AgNPs by *L. acidophilus*. The reduction of Ag+ by *L. acidophilus* (which possesses basic and electron-donating properties) led to the production of AgNPs. Absorbance Behavior at Different Ag+ Concentrations: At low Ag+ concentration (1 mM), the recorded absorbance of L. acidophilus-AgNPs decreased. This could be because nanoparticles did not form significantly at this concentration. Conversely, at higher Ag+ concentrations (4, 6, and 8 mM), the low absorbance values may be attributed to the toxic effect of Ag+ on cells, hindering NP formation. Interestingly, the SPR band intensity was higher at a concentration of 2 mM. This suggests that cells tolerated Ag+ better, resulting in increased AgNP production. Metal-Tolerance Bacteria and Nanoparticle Synthesis: Isolating metal-tolerant bacteria from metal-rich environments has been a focus in multiple studies. These bacteria have the potential to synthesize nanoparticles, including AgNPs (Jain *et al.,* 2013;Bhargava *et al.,* 2016). Our results shed light on the fascinating interplay between L. acidophilus, silver ions, and nanoparticle synthesis. Morphology and Size of L. acidophilus-AgNPs: The biosynthesized *L. acidophilus* -AgNPs exhibited uniform and spherical shapes. They were well dispersed without aggregation and had relatively smooth surfaces. Morphological examination confirmed the size values obtained by dynamic light scattering (DLS). Homogeneous Particle Size Distribution: The low polydispersity index (PDI) value of 0.54 indicated a homogeneous distribution of particle sizes. A high negative zeta potential of -9.55 ± 0.8 mV suggests that the nanovesicles repel each other, maintaining a stable colloidal dispersion

(Garmasheva *et al.,* 2016). This stability makes *L. acidophilus* -AgNPs suitable for oral drug delivery, especially as zeta potential decreases with increasing drug load (Król *et al.,* 2018;Tripathi *et al.,* 2014). UV-Vis Spectra and Absorption Bands: UV-vis spectra of *L. acidophilus* biomass typically show absorption maxima between 230 and 280 nm, attributed to proteins and polysaccharides. However, the UV-Vis absorption spectra of *L. acidophilus* -AgNPs displayed two distinct bands: At 245 nm (possibly related to specific functional groups). A prominent peak at 450 nm, corresponding to the surface plasmon resonance (SPR) band of *L. acidophilus* -AgNPs. This confirms the successful production of *L. acidophilus* -AgNPs (Hussein & Mohamed, 2010). FT-IR Spectral Analysis: When exposed to Ag+, the FT-IR spectra of *L. acidophilus* -AgNPs showed minimal changes in absorption peaks related to functional groups (-COOH, O-H, N-H, and (P=O, P-O)). These functional groups play a crucial role in binding Ag+ and facilitating the creation of *L. acidophilus* -AgNPs (Istek & Gurbuz, 2017).

Similar findings were reported in studies involving ZnO nanocomposites synthesized by other bacterial strains (Hussein, 2012; Król *et al.,* 2018;Tripathi *et al.,* 2014). According to our findings, there were 0, 1, 5, 7, 8, and 10 mortalities when *L. acidophilus* -AgNPs were given orally at dosages of 250, 500, 750, 1000, 1250, and 1500 mg/kg b.w., respectively. It was demonstrated that 850 mg/kg b.w. of *L. acidophilus* -AgNPs was the LD50 dosage required to kill 50% of mice. In the present investigation, we used *L. acidophilus*-AgNPs at concentrations of 14 and 42.5 mg/kg b.w., which corresponds to 1/20 and 1/50 LD50, respectively, to investigate the anti-obesity activity of *L. acidophilus* -AgNPs in HFD-fed mice. Several papers proved the induction of obesity in mice by feeding them a high-fat diet for eight weeks (Zhang *et al.,* 2019). *L. acidophilus*-AgNPs significantly reduced body weight in the high-fat diet-treated group. This unique anti-obesity effect could have therapeutic implications. Severe type II diabetes was observed in the high-fat diet group compared to regular diet-fed rats. Lipoprotein fractions containing apo-B contribute to cholesterol buildup in atherosclerotic lesions (Istek & Gurbuz, 2017). *L. acidophilus*-AgNPs regulated the production of liver TG, TC, HDL-C, and FFA. This mitigated hypercholesterolemia induced by the high-fat diet (Demori *et al.*, 2006; Thomàs-Moyà *et al.,* 2008). Changes in HMG-CoA reductase and cholesterol 7-hydroxylase activity likely contributed to reduced plasma cholesterol levels (Rozenberg & Aviram, 2006). Interestingly, *L. acidophilus*-AgNPs may enhance the activity of these enzymes, potentially lowering TG, TC, HDL-C, and FFA levels (Uzun *et al.,* 2007; Eldourghamy *et al.,* 2023). Our research sheds light on the promising role of *L. acidophilus*-AgNPs in managing obesity-related complications.

Our study confirms the findings of Huang et al., who found that *L. acidophilus* effectively reduced cholesterol levels in rats fed a high-cholesterol diet (Abou-Taleb *et al.,* 2021). Our article achieved this by suppressing the expression of NPC1L1 in the small intestine (Huang *et al.,* 2014). Chen and his team discovered that *L. acidophilus* reduced the severity of atherosclerotic plaques in mice lacking the ApoE gene (Chen *et al.,* 2013). On the other hand, the high-fat diet-administered group showed considerably high levels of hepatic TBARs (Metwaly et al., 2022; Elneklawi et al., 2023). Also, the levels of GSH, SOD, GPx, and GR showed significantly low levels in HFD-fed rats. Obese rats produce ROS, leading to organ oxidative damage, including the heart and liver (Botham & Wheeler-Jones, 2013; Mosaad *et al.,* 2022). *L. acidophilus* -AgNPs were shown to reduce ROS production and normalize the TBARs, GSH, SOD, GPx, and GR levels when administered to HFD-treated rats (Fayed et al., 2022; Naser Eldin et al., 2022). Supplementing with *L. acidophilus*-AgNPs helped the liver cells maintain antioxidant enzyme balance in HFD-treated rats.

Moreover, lipid peroxidation, which increases enzyme inactivation as well as the production of TNF-α and MCP-1, can be triggered by free radicals such as superoxide or H_2O_2 (Hussein, 2012). Our results provide evidence in favor of the theory that rats treated with HFD produced more inflammatory mediators due to the considerable increase in lipid peroxidation and cytokines. According to the present investigation, *L. acidophilus* -AgNPs may successfully reduce inflammation, which is reflected by decreased TNF-α and MCP-1 production, by scavenging free radicals, lowering lipid peroxidation, and increasing the synthesis of antioxidant enzymes.

The current findings align with El Gao et al.'s research (Gao *et al.,* 2022), which highlighted *L. acidophilus*'s ability to inhibit oxidative stress. This study introduces an eco-friendly method to synthesize silver nanoparticles using *Lactobacillus acidophilus,* which shows promise in treating obesity and its complications. The *L. acidophilus*-AgNPs exhibit strong antioxidants and anti-inflammatory

properties, crucial for managing obesity-induced oxidative stress. These findings highlight the potential of probiotic-derived nanoparticles in medical nanotechnology, particularly for chronic disease treatment. This research validates the probiotic benefits of *L. acidophilus* and its role in enhancing the efficacy of silver nanoparticles, paving the way for future clinical applications. Our histological examination revealed significant improvements in liver morphology following treatment with *Lactobacillus acidophilus*-AgNPs. In the HFD group, liver tissue exhibited moderate congestion, fatty changes, and inflammatory cell infiltration, consistent with previous studies demonstrating that high-fat diets induce hepatic steatosis and inflammation (Zhang et al., 2019; Huang et al., 2014). Treatment with *L. acidophilus*-AgNPs (42.5 mg/kg.b.w.) significantly reduced fatty changes and inflammatory cell infiltration, restoring hepatocyte morphology and sinusoid structure. These findings align with studies by Chen et al. (2013) and Gao et al. (2022), who reported that *L. acidophilus* supplementation ameliorates HFD-induced liver damage by reducing lipid accumulation and inflammation.

The reduction in fatty changes observed in our study (from 32.5 ± 3.2% in the HFD group to 12.4 ± 1.8% in the *L. acidophilus*-AgNPs-treated group) is comparable to the findings of Huang et al. (2014), who reported a similar reduction in hepatic lipid droplets following *L. acidophilus* administration. Additionally, the decrease in inflammatory cell infiltration (from 45.6 ± 5.3 cells/mm² in the HFD group to 18.7 ± 2.4 cells/mm² in the treated group) is consistent with the anti-inflammatory effects of *L. acidophilus* reported by Chen et al. (2013). The restoration of hepatocyte morphology and sinusoid structure in our study further supports the hepatoprotective effects of *L. acidophilus*-AgNPs. These findings agree with Gao et al. (2022), who demonstrated that *L. acidophilus* improves liver histology by modulating oxidative stress and inflammation. Overall, our histological results confirm the potential of *L. acidophilus*-AgNPs as a therapeutic agent for mitigating HFD-induced liver damage.

Limitations of the current study

While this study presents promising findings, it has several limitations, including a small sample size and short observation period, which may not fully capture long-term effects and potential side effects. The study's focus on high-fat diet-induced obesity in mice may limit the generalizability of the results to other models or humans. Additionally, the precise molecular mechanisms behind the observed benefits of *L. acidophilus* -AgNPs require further investigation. Translating these findings to human clinical applications poses significant challenges, including dosage optimization and safety assessments. Future research should address these limitations to validate and expand the therapeutic potential of *L. acidophilus* -AgNPs.

Mechanisms of Anti-Obesity Activity

The anti-obesity effects of *Lactobacillus acidophilus*-AgNPs observed in this study can be attributed to several mechanisms: Modulation of Lipid Metabolism: *L. acidophilus*-AgNPs significantly reduced plasma levels of total cholesterol (TC), triglycerides (TG), and free fatty acids (FFA), while increasing high-density lipoprotein cholesterol (HDL-C). This lipid-lowering effect is likely mediated by the upregulation of enzymes involved in lipid metabolism, such as HMG-CoA reductase and cholesterol 7-hydroxylase, as previously reported by Rozenberg & Aviram (2006). Additionally, *L. acidophilus*-AgNPs may enhance the excretion of bile acids, thereby reducing cholesterol absorption in the intestine, as demonstrated by Huang et al. (2014). Reduction of Oxidative Stress: *L. acidophilus*-AgNPs significantly increased the levels of antioxidant enzymes, including glutathione (GSH), superoxide dismutase (SOD), glutathione peroxidase (GPx), and glutathione reductase (GR), while reducing lipid peroxidation markers such as malondialdehyde (MDA). This antioxidant activity helps mitigate oxidative stress, which is a key contributor to obesity-related complications, as highlighted by Botham & Wheeler-Jones (2013). Anti-Inflammatory Effects: The administration of *L. acidophilus*-AgNPs significantly reduced the levels of pro-inflammatory cytokines, including tumor necrosis factor-alpha (TNF-α) and monocyte chemoattractant protein-1 (MCP-1), in the liver. This anti-inflammatory effect is consistent with previous studies showing that *L. acidophilus* suppresses inflammation by inhibiting the NF-κB signaling pathway, as reported by Chen et al. (2013). Improvement of Insulin Sensitivity: *L. acidophilus*-AgNPs significantly reduced plasma glucose and insulin levels, indicating improved insulin sensitivity. This effect may be mediated by the modulation of adiponectin and leptin levels, as suggested by Gao et al. (2022). Improved insulin sensitivity helps regulate lipid metabolism and reduces fat accumulation in adipose tissue.

Restoration of Gut Microbiota Balance: Probiotics such as *L. acidophilus* are known to restore gut microbiota balance, which plays a crucial role in regulating energy metabolism and body weight. By promoting the growth of beneficial bacteria and inhibiting pathogenic species, *L. acidophilus*-AgNPs may enhance gut barrier function and reduce systemic inflammation, as demonstrated by Huang et al. (2014).

CONCLUSIONS

This experiment successfully demonstrated the production of *L. acidophilus* -AgNPs using *L. acidophilus* biomass. The characterization of *L. acidophilus* included bile salt tolerance assays, cell-surface adherence tests, hemolytic tests, 16S rDNA sequencing, and agarose gel electrophoresis of PCR-amplified products. The MTC results indicated that 2 mM of Ag+ is the optimal concentration for producing *L. acidophilus* -AgNPs. These nanoparticles, generated through biological processes, were spherical with an average size of 18.69 ± 0.57 nm and a PDI of 0.54. The zeta potential was -9.55 ± 0.8 mV. UV-visible and FTIR spectrum data revealed the presence of OH, C=O, NH, P-O, and P=O functional groups in the proteins and polysaccharides of *L. acidophilus*. Additionally, the biosynthesized *L. acidophilus* -AgNPs exhibited significant lipid-lowering, antioxidant, and anti-inflammatory properties in mice with high-fat diet-induced obesity. The synthesis of *L. acidophilus* -AgNPs is both ecologically sound and economically viable, acting as a microbial cell nanofactory. Future research should focus on thoroughly analyzing the physicochemical characteristics of these biosynthesized nanoparticles and exploring their additional biological applications.

ABBREVIATIONS

Triacylglycerols (TG), total cholesterol (TC), free fatty acids (FFA), reduced glutathione (GSH), superoxide dismutase (SOD), glutathione peroxidase (GPx), glutathione reductase (GR), malondialdehyde (MDA), tumor necrosis factor-alpha (TNF-α), and monocyte chemoattractant protein-1 (MCP-1).

AUTHORS' CONTRIBUTIONS

All authors contributed significantly to the work reported, whether in the study design, and biological analysis, or all of these areas; participated in drafting, revising, or critically reviewing the article; gave final approval of the version to be published; agreed on the journal to which the article was submitted; and agreed to be accountable for all aspects of the work.

ETHICAL COMMITTEE APPROVAL

All experiment methods were carried out under ethical standards and per a protocol authorized by the Ethics Committee of the Faculty of Applied Health Sciences, October 6 University in Egypt (No. 20221005)

POTENTIAL CONFLICTS OF INTEREST

There are no conflicts of interest reported by any of the writers concerning this work.

AVAILABILITY OF DATA AND MATERIALS

The data supporting the findings of the article is available within the article.

REFERENCES

Abal Camaño, P., Louzao Ojeda, M. C., Antelo Queijo, Á., Alvarez, M., Cagide, E., Vilariño del Río, N., Rodríguez Vieytes, M. M., & Botana López, L. M. 2017. "Acute Oral Toxicity of Tetrodotoxin in Mice: Determination of Lethal Dose 50 (LD50) and No Observed Adverse Effect Level (NOAEL)."

Abdalla, M., Kasser, A. K., & Mohammed, A. B. 2023. "Isolation of Lactobacillus HBUAS56719 from Black Raspberry Leaves and its In-vitro Antidiabetic Activity." Research Journal of Applied Biotechnology 9 (1): 14–27.

Abou-Taleb, N. A., Elblasy, O. A., Elbesoumy, E. A., Basuny, H. I., Elhamadi, E. A., Nasreldin, M. S., Emare, A. A., Ali, A. A., Salem, M. A., Ahmed, F. M., & Hussein, M. A. 2021. "Mechanism of Antiangiogenic and Antioxidant Activity of Newly Synthesized CAMBA in Ehrlich Ascites Carcinoma-Bearing Mice." Asian Journal of Chemistry 33: 2465-2471.

Alamir, M., Hussein, M. A., Aboud, H. M., Khedr, M. H., & Zanaty, M. I. 2024. "Optimization of Phloretin-loaded Nanospanlastics for Targeting of FAS/SREBP1c/AMPK/OB-Rb Signaling Pathway in HFD-induced Obesity." Current Pharmaceutical Biotechnology.

Allain, C. C., Poon, L. S., Chan, C. S. G., Richmond, W., & Fu, P. C. 1974. "Enzymatic Determination of Total Serum Cholesterol." Clinical Chemistry 20 (4): 470–475.

Al-nami, S. Y., Alorabi, A. O., Al-Ahmed, Z. A., Mogharbel, A. T., Abumelha, H. M., Hussein, M. A., & El-Metwaly, N. 2023. "Superficial and Inkjet Scalable Printed Sensors Integrated with Iron Oxide and Reduced Graphene Oxide for Sensitive Voltametric Determination of Lurasidone." ACS Omega 8 (11): 10449–10458.

Al-Nami, S. Y., Alorabi, A. Q., Al-Ahmed, Z. A., Mogharbel, A. T., Abumelha, H. M., Hussein, M. A., & El-Metwaly, N. M. 2023. "Superficial and Inkjet Scalable Printed Sensors Integrated with Iron Oxide and Reduced Graphene Oxide for Sensitive Voltammetric Determination of Lurasidone." ACS Omega 8 (11): 10449–10458.

Altermann, E., Russell, W. M., Azcarate-Peril, M. A., Barrangou, R., Buck, B. L., McAuliffe, O., Souther, N., Dobson, A., Duong, T., & Callanan, M. 2005. "INAUGURAL ARTICLE by a Recently Elected Academy Member: Complete Genome Sequence of the Probiotic Lactic Acid Bacterium *Lactobacillus acidophilus* NCFM." Proceedings of the National Academy of Sciences of the United States of America 102 (11): 3906.

Azcarate-Peril, M. A., Altermann, E., Hoover-Fitzula, R. L., Cano, R. J., & Klaenhammer, T. R. 2004. "Identification and Inactivation of Genetic Loci Involved with Lactobacillus *acidophilus* Acid Tolerance." Applied and Environmental Microbiology 70 (9): 5315–5322.

Bhargava, A., Jain, N., Khan, M. A., Pareek, V., Dilip, R. V., & Panwar, J. 2016. "Utilizing Metal Tolerance Potential of Soil Fungus for Efficient Synthesis of Gold Nanoparticles with Superior Catalytic Activity for Degradation of Rhodamine B." Journal of Environmental Management 183: 22–32.

Borik, R. M., & Hussein, M. A. 2021. "Synthesis, Molecular Docking, Biological Potentials and Structure-activity Relationship of New Quinazoline and Quinazoline-4-one Derivatives." Asian J Chem 33 (2): 423-438.

Borik, R. M., & Hussein, M. A. 2022. "A Novel Quinazoline-4-one Derivatives as a Promising Cytokine Inhibitors: Synthesis, Molecular Docking, and Structure-Activity Relationship." Current Pharmaceutical Biotechnology 23 (9): 1179–1203.

Boshra, S. A., & Hussein, M. A. 2016. "Cranberry Extract as a Supplemented Food in Treatment of Oxidative Stress and Breast Cancer Induced by N-Methyl-N-Nitrosourea in Female Virgin Rats." International Journal of Phytomedicine 8 (2): 217–227.

Botham, K. M., & Wheeler-Jones, C. P. D. (2013). "Postprandial Lipoproteins and the Molecular Regulation of Vascular Homeostasis." *Progress in Lipid Research*, 52(4), 446–464. https://doi.org/10.1016/j.plipres.2013.06.001 Chen, L., Liu, W., Li, Y., Luo, S., Liu, Q., Zhong, Y., Jian, Z., & Bao, M. (2013). "Lactobacillus acidophilus ATCC 4356 Attenuates the Atherosclerotic Progression through Modulation of Oxidative Stress and Inflammatory Process." *International Immunopharmacology*, 17(1), 108–115. https://doi.org/10.1016/j.intimp.2013.05.018

Botham, K. M., & Wheeler-Jones, C. P. D. 2013. "Postprandial Lipoproteins and the Molecular Regulation of Vascular Homeostasis." Progress in Lipid Research 52 (4): 446–464.

Carleton, H. M., & Drury, R. A. B. 1980. "Carleton's Histological Technique." 5th ed. Wallington, New York, Oxford. 1–200.

Chen, L., Liu, W., Li, Y., Luo, S., Liu, Q., Zhong, Y., Jian, Z., & Bao, M. 2013. "Lactobacillus acidophilus ATCC 4356 Attenuates the Atherosclerotic Progression through Modulation of Oxidative Stress and Inflammatory Process." International *Immunopharmacology* 17 (1): 108–115.

Claesson, M. J., Van Sinderen, D., & O'Toole, P. W. 2007. "The Genus Lactobacillus—a Genomic Basis for Understanding its Diversity." FEMS Microbiology Letters 269 (1): 22–28.

Demori, I., Voci, A., Fugassa, E., & Burlando, B. 2006. "Combined Effects of High-fat Diet and Ethanol Induce Oxidative Stress in Rat Liver." Alcohol 40 (3): 185–191.

Dym, O., & Eisenberg, D. 2001. "Sequence-structure Analysis of FAD-containing Proteins." Protein Science 10 (9): 1712–1728.

Eldourghamy, A., Hossam, T., Hussein, M. A., Abdel-Aziz, A., & Samir, A. E. 2023. "Naringenin Suppresses NLRP3 Inflammasome Activation via the mRNA-208a Signaling Pathway in Isoproterenol-induced Myocardial Infarction." Asian Pacific Journal of Tropical Biomedicine 13 (10): 443-450. doi: 10.4103/2221-1691.387750.

El-Gizawy, H. A. E., & Hussein, M. A. 2015. "Fatty Acids Profile, Nutritional Values, Anti-diabetic and Antioxidant Activity of the Fixed Oil of Malva parviflora Growing in Egypt." *Int. J. Phytomed.,* 7; 219-230.

Elharrif, M. G., Abdel Maksoud, H. A., Abdullah, M. H., & Abd Elmohsen, A. S. 2024. "Biochemical Evaluation of Possible Protective Effect of Purslane Extract in Experimentally Induced Arthritis Associated with Obesity." Prostaglandins Other Lipid Mediat 172: 106823. doi: 10.1016/j.prostaglandins.2024.106823.

Elneklawi, M. S., Mohamed, Z. N., Hussein, M. A., & Mohamad, E. A. 2023. "STEN Ameliorates VEGF Gene Expression by Improving XBP1/mRNA-21/mRNA-330 Signalling Pathways in Cisplatin-induced Uterus Injury in Rats." Journal of Drug Delivery Science and Technology 87: 104760. doi: 10.1016/j.jddst.2023.104760.

Fayed, A. M., Abdalla, E. A., Hassan, S. A., Hussein, M. A., & Roshdy, T. M. 2022. "Downregulation of TLR4-NF-kB-p38 MAPK Signalling in Cholestatic Rats Treated with Cranberry Extract." Pak J Biol Sci 25 (2): 112-122. doi: 10.3923/pjbs.2022.112.122.

Fossati, P., & Prencipe, L. 1982. "Serum Triglycerides Determined Colorimetrically with an Enzyme that Produces Hydrogen Peroxide." Clinical Chemistry 28 (10): 2077–2080.

Gao, H., Li, X., Chen, X., Hai, D., Wei, C., Zhang, L., & Li, P. 2022. "The Functional Roles of Lactobacillus acidophilus in Different Physiological and Pathological Processes." Journal of Microbiology and Biotechnology 32 (10): 1226.

Gao, H., Li, X., Chen, X., Hai, D., Wei, C., Zhang, L., & Li, P. (2022). "The Functional Roles of Lactobacillus acidophilus in Different Physiological and Pathological Processes." *Journal of Microbiology and Biotechnology*, 32(10), 1226–1238. https://doi.org/10.4014/jmb.2205.05010 Huang, Y., Wang, J., Quan, G., Wang, X., Yang, L., & Zhong, L. (2014). "Lactobacillus acidophilus ATCC 4356 Prevents Atherosclerosis via Inhibition of Intestinal Cholesterol Absorption in Apolipoprotein E-Knockout Mice."

Applied and Environmental Microbiology, 80(24), 7496–7504. https://doi.org/10.1128/AEM.02926-14

Garmasheva, I., Kovalenko, N., Voychuk, S., Ostapchuk, A., Livins'ka, O., & Oleschenko, L. 2016. "Lactobacillus Species Mediated Synthesis of Silver Nanoparticles and Their Antibacterial Activity Against Opportunistic Pathogens in Vitro." BioImpacts: BI 6 (4): 219.

Gobba, N. A. E. K., Hussein Ali, A., El Sharawy, D. E., & Hussein, M. A. 2018. "The Potential Hazardous Effect of Exposure to Iron Dust in Egyptian Smoking and Nonsmoking Welders." Archives of Environmental & Occupational Health 73 (3): 189–202.

Huang, Y., Wang, J., Quan, G., Wang, X., Yang, L., & Zhong, L. 2014. "Lactobacillus acidophilus ATCC 4356 Prevents Atherosclerosis via Inhibition of Intestinal Cholesterol Absorption in Apolipoprotein E-Knockout Mice." Applied and Environmental Microbiology 80 (24): 7496–7504.

Hussein, M. A. 2012. "Synthesis of Some Novel Triazoloquinazolines and Triazinoquinazolines and Their Evaluation for Anti-inflammatory Activity." Med Chem Res 21: 1876–1886. doi: 10.1007/s00044-011-9707-0.

Hussein, M. A. 2021. "Administration of Exogenous Surfactant and Cytosolic Phospholipase A2α Inhibitors May Help COVID-19 Infected Patients with Chronic Diseases." Coronaviruses 2 (12): 7–26.

Hussein, M. A., & Boshra, S. 2013. "Antitumor and Structure Antioxidant Activity Relationship of Colchicine on Ehrlich Ascites Carcinoma (EAC) in Female Mice." International Journal of Drug Delivery 5 (4): 430–437.

Hussein, M. A., & Mohamed, A. G. S. 2010. "In Vivo Hepato-protective Properties of Purslane Extracts on Paracetamol-Induced Liver Damage." Malays J Nutr 16 (1): 161-70. PMID: 22691863.

Hussein, M. A., Borik, R. M., Nafie, M. S., Abo-Salem, H. M., Boshra, S. A., & Mohamed, Z. N. 2023. "Structure Activity Relationship and Molecular Docking of Some Quinazolines Bearing Sulfamerazine Moiety as New 3CLpro, cPLA2, sPLA2 Inhibitors." Molecules 28 (16): 6052. doi: 10.3390/molecules28166052.

Hussein, M. A., Mohammad, S. I., Ali, A. A., Mohamed, S. M., Mohamed, B., Mohamed, A. S., Ahmed, S. A., & El Gizawy, H. A. 2024. "Malva parviflora Seed Oil; Isolation, Gas Chromatographic Profiling and Its Cardioprotective Activity Against Myocardial Infraction in Animal Model." Journal of King Saud University–Science 36: 1018-364. doi: 10.1016/j.jksus.2023.103060.

Hussein, M.A. 2012. Synthesis of some novel triazoloquinazolines and triazinoquinazolines and their evaluation for anti-inflammatory activity. *Med Chem Res* 21: 1876–1886. https://doi.org/10.1007/s00044-011-9707-0

Hussein, M.A., Abdel-Gawad, S.M. 2010. Protective effect of Jasonia montana against ethinylestradiol-induced cholestasis in rats. Saudi Pharm J. 18(1): 27-33. doi: 10.1016/j.jsps.2009.12.002.

Istek, N., & Gurbuz, O. 2017. "Investigation of the Impact of Blueberries on Metabolic Factors Influencing Health." Journal of Functional Foods 38: 298–307.

Jain, N., Bhargava, A., Tarafdar, J. C., Singh, S. K., & Panwar, J. 2013. "A Biomimetic Approach Towards Synthesis of Zinc Oxide Nanoparticles." Applied Microbiology and Biotechnology 97: 859–869.

Kakkar, P., Das, B., & Viswanathan, P. N. 1984. "A Modified Spectrophotometric Assay of Superoxide Dismutase." Indian Journal of Biochemistry & Biophysics 21 (2): 130–132.

Kalimuthu, K., Babu, R. S., Venkataraman, D., Bilal, M., & Gurunathan, S. 2008. "Biosynthesis of Silver Nanocrystals by Bacillus licheniformis." Colloids and Surfaces B: Biointerfaces 65 (1): 150–153.

Kamal, G., Nasr, M., Hussein, M. A., Abdel-Aziz, A., & Fayed, A. M. 2022. "Morin: A Promising Nutraceutical Therapy for Modulation of the NF-κB/NOX-2/IL-6/HO-1 Signaling Pathways in Paracetamol-induced Liver Toxicity." Biomedical Research and Therapy 9 (9): 5260-5271.

Król, A., Railean-Plugaru, V., Pomastowski, P., Złoch, M., & Buszewski, B. 2018. "Mechanism Study of Intracellular Zinc Oxide Nanocomposites Formation." Colloids and Surfaces A: Physicochemical and Engineering Aspects 553: 349–358.

Leite, A. M. O., Miguel, M. A. L., Peixoto, R. S., Ruas-Madiedo, P., Paschoalin, V. M. F., Mayo, B., & Delgado, S. 2015. "Probiotic Potential of Selected Lactic Acid Bacteria Strains Isolated from Brazilian Kefir Grains." Journal of Dairy Science 98 (6): 3622–3632.

Maiorino, F. M., Brigelius-Flohé, R., Aumann, K. D., Roveri, A., Schomburg, D., & Flohé, L. 1995. "[5] Diversity of Glutathione Peroxidases." In Methods in Enzymology, Vol. 252, 38–53. Elsevier.

Markus, J., Mathiyalagan, R., Kim, Y.-J., Abbai, R., Singh, P., Ahn, S., Perez, Z. E. J., Hurh, J., & Yang, D. C. 2016. "Intracellular Synthesis of Gold Nanoparticles with Antioxidant Activity by Probiotic Lactobacillus kimchicus DCY51T Isolated from Korean Kimchi." Enzyme and Microbial Technology 95: 85–93.

Metwaly, A. M., Elmoghazy, H. M., Hussein, M. A., Abdel-ziz, A., & Elmasry, S. A. 2022. "CAPE Improves Vanin-1/AKT/miRNA-203 Signaling Pathways in DSS Induced Ulcerative Colitis." Biomed Res Ther 9 (9): 5313-5325.

Mohamad, E. A., Mohamed, Z. N., Hussein, M. A., & Elneklawi, M. S. 2022. "GANE Can Improve Lung Fibrosis by Reducing Inflammation via Promoting p38MAPK/TGF-β1/NF-κB Signaling Pathway Downregulation." ACS Omega 7 (3): 3109–3120.

Mosaad, Y. O., Baraka, M. A., Warda, A. E. A., Ateyya, H., Hussein, M. A., & Gaber, S. 2022. "Plasma Lipid Profile: A Predictive Marker of Disease Severity Among COVID-19 Patients—An Opportunity for Low-income Countries." Drugs Ther Perspect 38 (6): 286-291. doi: 10.1007/s40267-022-00916-8.

Mosaad, Y. O., Hussein, M. A., Ateyya, H., Mohamed, A. H., Ali, A. A., Ramadan Youssuf, A., Wink, M., & El-Kholy, A.

A. 2022. “Vanin 1 Gene Role in Modulation of iNOS/MCP-1/TGF-β1 Signaling Pathway in Obese Diabetic Patients.” Journal of Inflammation Research: 6745–6759.

Naser Eldin, M. S., Eissa, M. T., Mansour, M. T., Abdelmonem, H. A., Ahmed, A. A., Ali, N. O., Abd El-haleem, M. A., Sayed, S. A., Emara, S. M., Yousif, M. M., Ibrahim, M. A., Salem, M. A., Ahmed, F. M., & Hussein, M. A. 2022. “Green Synthesis of Purslane Seeds-Selenium Nanoparticles and Evaluate Its Cytokines Inhibitor in Lead Acetate Induced Toxicity in Rats.” Asian Journal of Chemistry 4: 894-900. doi: 10.14233/ajchem.2022.23362.

Organization, W.H. 2022. https://www.who.int/news-room/fact-sheets/detail/obesity-and-overweight. Accessed.

Owen, J. B., & Butterfield, D. A. 2010. “Measurement of Oxidized/Reduced Glutathione Ratio.” Protein Misfolding and Cellular Stress in Disease and Aging: Concepts and Protocols: 269–277.

Panáček, A., Kvitek, L., Prucek, R., Kolář, M., Večeřová, R., Pizúrová, N., Sharma, V. K., Nevěčná, T., & Zbořil, R. 2006. “Silver Colloid Nanoparticles: Synthesis, Characterization, and Their Antibacterial Activity.” The Journal of Physical Chemistry B 110 (33): 16248–16253.

Roa, M., Blane, K., & Zonneberg, M. 1985. “One Way Analysis of Variance. Version IA (C); PC-STAT, Program Coded by University of Georgia: USA.”

Rozenberg, O., & Aviram, M. (2006). "S-Glutathionylation Regulates HDL-Associated Paraoxonase 1 (PON1) Activity." *Biochemical and Biophysical Research Communications*, 351(2), 492–498. https://doi.org/10.1016/j.bbrc.2006.10.056

Rozenberg, O., & Aviram, M. 2006. “S-Glutathionylation Regulates HDL-Associated Paraoxonase 1 (PON1) Activity.” Biochemical and Biophysical Research Communications 351 (2): 492–498.

Sahar Abbasiliasi, S. A., Tan JooShun, T. J., Fatemeh Bashokouh, F. B., Tengku Azmi, T. I., Shuhaimi Mustafa, S. M., Faezeh Vakhshiteh, F. V., Subhashini Sivasamboo, S. S., & Ariff, A. B. 2017. “In Vitro Assessment of Pediococcus acidilactici Kp10 for Its Potential Use in the Food Industry.”

Salah, A., Mohammed El-Laban, N., Mafiz Alam, S., Shahidul Islam, M., Abdalla Hussein, M., & Roshdy, T. 2024. “Optimization of Naringenin-loaded Nanoparticles for Targeting of Vanin-1, iNOS, and MCP-1 Signaling Pathway in HFD-induced Obesity.” Int J Pharm 654: 123967. doi: 10.1016/j.ijpharm.2024.123967.

Shehata, M. R., Mohamed, M. M. A., Shoukry, M. M., Hussein, M. A., & Hussein, F. M. 2015. “Synthesis, Characterization, Equilibria and Biological Activity of Dimethyltin (IV) Complex with 1,4-Piperazine.” Journal of Coordination Chemistry 68 (6): 1101–1114.

Soliman, S. M., Mosallam, S., Mamdouh, M. A., Hussein, M. A., & Abd El-Halim, S. M. 2022. “Design and Optimization of Cranberry Extract Loaded Bile Salt Augmented Liposomes for Targeting of MCP-1/STAT3/VEGF Signaling Pathway in DMN-Intoxicated Liver in Rats.” Drug Delivery 29 (1): 427–439.

Thomas, R., Janardhanan, A., Varghese, R. T., Soniya, E. V., Mathew, J., & Radhakrishnan, E. K. 2014. “Antibacterial Properties of Silver Nanoparticles Synthesized by Marine Ochrobactrum sp.” Brazilian Journal of Microbiology 45: 1221–1227.

Thomàs-Moyà, E., Gómez-Pérez, Y., Fiol, M., Gianotti, M., Lladó, I., & Proenza, A. M. 2008. “Gender Related Differences in Paraoxonase 1 Response to High-fat Diet-induced Oxidative Stress.” Obesity 16 (10): 2232–2238.

Tripathi, R. M., Bhadwal, A. S., Gupta, R. K., Singh, P., Shrivastav, A., & Shrivastav, B. R. 2014. “ZnO Nanoflowers: Novel Biogenic Synthesis and Enhanced Photocatalytic Activity.” Journal of Photochemistry and Photobiology B: Biology 141: 288–295.

Tsikas, D. 2017. “Assessment of Lipid Peroxidation by Measuring Malondialdehyde (MDA) and Relatives in Biological Samples: Analytical and Biological Challenges.” Analytical Biochemistry 524: 13–30.

Uzun, H., Konukoglu, D., Gelisgen, R., Zengin, K., & Taskin, M. 2007. “Plasma Protein Carbonyl and Thiol Stress Before and After Laparoscopic Gastric Banding in Morbidly Obese Patients.” Obesity Surgery 17: 1367–1373.

Zhang, Y., Li, X., Zhang, H., Zhao, Y., & Chen, Y. (2019). "Lactobacillus acidophilus Ameliorates Obesity in High-Fat Diet-Induced Mice by Regulating Gut Microbiota and Lipid Metabolism." *Journal of Functional Foods*, 52, 243–251. https://doi.org/10.1016/j.jff.2018.11.008.